KECK/MOSFIRE SPECTROSCOPIC CONFIRMATION[*] OF A VIRGO-LIKE CLUSTER ANCESTOR AT $z = 2.095$

Tiantian Yuan[1], Themiya Nanayakkara[2], Glenn G. Kacprzak[2,8], Kim-Vy H. Tran[3], Karl Glazebrook[2],
Lisa J. Kewley[1], Lee R. Spitler[4,5], Gregory B. Poole[6], Ivo Labbé[7], Caroline M. S. Straatman[7], and Adam R. Tomczak[3]

[1] Research School of Astronomy and Astrophysics, The Australian National University, Cotter Road, Weston Creek, ACT 2611, Australia
[2] Centre for Astrophysics and Supercomputing, Swinburne University, Hawthorn, VIC 3122, Australia
[3] George P. and Cynthia Woods Mitchell Institute for Fundamental Physics and Astronomy, and Department of Physics and Astronomy,
Texas A&M University, College Station, TX 77843-4242, USA
[4] Department of Physics and Astronomy, Macquarie University, Sydney, NSW 2109, Australia
[5] Australian Astronomical Observatory, P.O. Box 296, Epping, NSW 1710, Australia
[6] School of Physics, University of Melbourne, Parksville, VIC 3010, Australia
[7] Sterrewacht Leiden, Leiden University, NL-2300 RA Leiden, The Netherlands

ABSTRACT

We present spectroscopic confirmation of a galaxy cluster at $z = 2.095$ in the COSMOS field. This galaxy cluster was first reported in the ZFOURGE survey as harboring evolved massive galaxies using photometric redshifts derived with deep near-infrared (NIR) medium-band filters. We obtain medium-resolution ($R \sim 3600$) NIR spectroscopy with MOSFIRE on the Keck 1 telescope and secure 180 redshifts in a $12' \times 12'$ region. We find a prominent spike of 57 galaxies at $z = 2.095$ corresponding to the galaxy cluster. The cluster velocity dispersion is measured to be $\sigma_{\rm v1D} = 552 \pm 52$ km s^{-1}. This is the first study of a galaxy cluster in this redshift range ($z \gtrsim 2.0$) with the combination of spectral resolution (~ 26 km s^{-1}) and the number of confirmed members (>50) needed to impose a meaningful constraint on the cluster velocity dispersion and map its members over a large field of view. Our ΛCDM cosmological simulation suggests that this cluster will most likely evolve into a Virgo-like cluster with $M_{\rm vir} = 10^{14.4 \pm 0.3} M_{\odot}$ (68% confidence) at $z \sim 0$. The theoretical probability of finding such a cluster is $\sim 4\%$. Our results demonstrate the feasibility of studying galaxy clusters at $z > 2$ in the same detailed manner using multi-object NIR spectrographs as has been done in the optical in lower-redshift clusters.

Key words: galaxies: clusters: general – galaxies: high-redshift – large-scale structure of universe

Online-only material: color figures

1. INTRODUCTION

In the standard cosmological model of structure formation, galaxy clusters are the largest collapsing structures located at the nodes of the cosmic web. Studies of local galaxies have found strong correlations of galaxy properties with the environment (e.g., Dressler 1980; Hogg et al. 2004). However, it is largely unknown whether and how these correlations would hold up at higher redshifts of $z \gtrsim 2$, when the mean star formation activities of the universe peaked and clusters were formed (e.g., Hopkins & Beacom 2006; Rettura et al. 2010). Studying dense galaxy groups and clusters at $z \gtrsim 2$ provides crucial knowledge of the star formation history of high-mass galaxies and the hierarchical growth of massive structures (e.g., McCarthy et al. 2007; Tran et al. 2010; Stanford et al. 2012; Zeimann et al. 2012; Brodwin et al. 2013; Strazzullo et al. 2013; Henry et al. 2014).

Great progress has been made in increasing the number of cluster candidates at $z \gtrsim 1.6$ (e.g., Papovich et al. 2010; Hayashi et al. 2012; Muzzin et al. 2013; Lee et al. 2014; Chiang et al. 2014; Newman et al. 2014). To secure the identification of a cluster, and to further elucidate the star formation history and physical properties of the galaxy members, spectroscopic follow-up is necessary. Due to the amount of large telescope time required, it is not surprising that to date only a handful of spectroscopically confirmed galaxy clusters with developed red sequences are known at $z \gtrsim 2$. Existing studies either do not have accurate cluster velocity dispersion measurements due to small numbers (<10) resulting in large uncertainties (Kurk et al. 2004; Galametz et al. 2013), or membership comes from *Hubble Space Telescope* (*HST*) grism redshifts with typical redshift accuracies of ± 200 km s^{-1} on individual galaxies (Gobat et al. 2013). Non-uniform redshift identifications from different instruments with limited spectral resolution and sensitivity also makes it difficult to quantify the errors of cluster velocity dispersion (Shimakawa et al. 2014).

We capitalize on the efficient Multi-Object Spectrometer for InfraRed Exploration (MOSFIRE; McLean et al. 2010, 2012) on KECK-1 to carry out a uniform spectroscopic survey on a galaxy cluster at $z \sim 2$ (Spitler et al. 2012) that was first identified using deep medium-band photometry in the FourStar (Persson et al. 2013) Galaxy Evolution Survey (ZFOURGE[9]) as having a striking overdensity in red galaxies. In this Letter, we use MOSFIRE to spectroscopically confirm 57 cluster members (spectral resolution ~ 10 km s^{-1}) and accurately measure the galaxy cluster's velocity dispersion. Our study also confirms the robustness of the ZFOURGE photometric redshifts and our ability to detect galaxies at $z \gtrsim 2$.

Throughout the Letter, we adopt a flat cosmology with $\Omega_M = 0.3$, $\Omega_\Lambda = 0.7$, and $H_0 = 70$ km s^{-1} Mpc^{-1}. At the cluster redshift of $z = 2.09$, 10 arcmin corresponds to an angular scale of 5 Mpc in proper coordinates.

---

[9] http://zfourge.tamu.edu

2. SPECTROSCOPIC OBSERVATIONS

2.1. MOSFIRE Sample Selection and Observations

We select spectroscopic targets based on the photometric redshifts in ZFOURGE that were derived from imaging in deep near-infrared (NIR) medium-band filters (Spitler et al. 2012, 2014). The $z \sim 2$ galaxy cluster candidate was first discovered within the COSMOS field in a single pointing of $\sim 11' \times 11'$ targeted by ZFOURGE (Spitler et al. 2012). The median uncertainties for the ZFOURGE photometry is ~ 0.05 dex (Tomczak et al. 2014), sufficient to allow for efficient cluster member candidates selection.

We obtained the spectroscopic data on MOSFIRE on the KECK 1 telescope on Mauna Kea. We conducted our observations on 2013 December 24–25 and 2014 February 10–13 with the aim of (1) securing as many redshifts as possible in the field of the cluster candidate and (2) obtaining high signal-to-noise ratio (S/N) spectra to study the physical properties (e.g., mass–metallicity relation; G. G. Kacprzak et al., in preparation) of the cluster members. We configured eight masks in the K-band filter covering 1.93–2.45 μm (sensitive for detecting Hα and [N II] lines at $z \sim 2$), and two masks in the H-band filter covering 1.46–1.81 μm (sensitive for detecting Hβ and [O III] lines at $z \sim 2$). We use a $0.''7$ slit width which yields a spectral resolution of $R = 3690$ in the K band and $R = 3620$ in the H band.

Taking advantage of the $6.'1 \times 6.'1$ MOSFIRE field of view, we targeted 224 objects in six pointings and secured redshifts for 180 objects. The total on-source exposure time for the K-band masks is ~ 2 hr each. For the two H-band masks, the exposure is 5.3 and 3.2 hr, respectively. The observing conditions were excellent for most of our masks, with seeing FWHM varying from $\simeq 0.''4$ to $\simeq 0.''7$. An A0V type standard star was observed in both the wide-slit mode and the narrow-science-slit ($0.''7$ slit width) mode before and after our science targets. The standard stars are used for telluric and flux calibration.

2.2. Data Reduction and Redshift Measurements

The raw MOSFIRE data were reduced using the publicly available data reduction pipeline (DRP) developed by the instrument team[10] available at the time. The output of the MOSFIRE DRP were background-subtracted, rectified, and wavelength calibrated two-dimensional spectra (see Figure 1). All spectra were calibrated to vacuum wavelengths. The typical residual for the wavelength solution is $\lesssim 0.1$ Å.

Similar to the procedure used in Steidel et al. (2014), we develop our own IDL routines to implement the telluric correction and flux calibration based on the standard stars. The one-dimensional (1D) spectrum and its associated 1σ error spectrum are extracted using an aperture that corresponds to the FWHM of the spatial profile of the well detected object (S/N > 5). For objects that are too faint to fit a Gaussian spatial profile, we use the FWHM of the stellar profile on the same mask as the extraction aperture.

Gaussian profiles were fit simultaneously to user-defined emission lines, e.g., Hα and [N II], with the line center and velocity width constrained to be the same within a given K band or H band. Most of our targets can be well fit by a single Gaussian component in the spectral direction. However, some of the galaxies in our sample have good resolved velocity structures in the emission lines due to great seeing (e.g., bottom left panel

_____
[10] See http://code.google.com/p/mosfire/.

in Figure 1). Those spectra require multiple component fitting and will be presented in our future kinematic work of the sample. The output of the code includes redshift, line flux, line width, and the associated errors. The statistical errors for each parameter are estimated using the 1σ error spectrum of the DRP, which we have tested to represent the correct level of variation of the spectrum.

Examples of our reduced MOSFIRE spectra are presented in Figure 1. We show four cluster galaxies of different brightness and spectral quality that are representative of our whole sample. The K-band magnitude (AB) range of our cluster galaxies is $20.8 \leqslant Ks \leqslant 26.1$ with a median value of 23.86 (T. Nanayakkara et al., in preparation). The faintest objects that we have detected emission lines (S/N > 5) have $Ks \sim 25$.

We flag the final redshifts in three categories based on the reliability of the redshift identification and measurements.

1. For objects with at least two emission lines identified at S/N > 5, we flag them as "$Q_z = 3$," meaning the quality of the redshift are the highest and we are confident that the line identification and redshift measurement are correct.

2. For objects that show only one emission line with S/N > 5, we assign them as "$Q_z = 2$" redshifts. The general match of the "$Q_z = 2$" object redshifts with their photometric redshifts suggests that the single line identification is most likely to be correct (see Figure 2). The "$Q_z = 2$" objects also show a spike at the cluster redshift, further validating the "$Q_z = 2$" redshifts (Figure 3). The rms scatter between our spectroscopic redshifts and the ZFOURGE photometric redshifts is about 5% (Figure 1).

3. For objects that have no obvious line detection (i.e., S/N < 5), we assign them as "$Q_z = 1$" redshifts and do not include them in the spec-z sample.

In summary, we identify 150 $Q_z = 3$ objects, 30 $Q_z = 2$ objects, and 44 $Q_z = 1$ objects ranging from spectroscopic $z \sim 1.9$ to 3.0. The statistical errors determined from the fit to Gaussian centroids for $Q_z = 2$ and $Q_z = 3$ redshifts are in the range of $\Delta z \sim 0.0001$–0.0002 (median = 0.00008). To examine the systematic uncertainties, we compare the redshifts of the $Q_z = 3$ objects ($N \sim 40$) that have redundant observations with S/N $\geqslant 10$ in both the K and H bands. The agreement between the redundantly detected redshifts is Δz(median) = 0.00005 and Δz(rms) = 0.00078. We thus quote Δz(rms) = $0.00078/\sqrt{2}$ = 0.00055 as the total uncertainty of our redshift measurement, which is contributed mostly from systematic uncertainties. At $z = 2.1$, this error corresponds to a rest-frame velocity uncertainty of Δv(rms) = 53 km s^{-1} (spectral resolution ~ 26 km s^{-1}).

3. RESULTS

3.1. Redshifts and Cluster Velocity Dispersion

We show in Figure 3 the histogram of the spectroscopic redshifts for $Q_z = 3$ (red) and $Q_z = 2$ objects (black). The redshift range of $2.0 < z < 2.3$ are used to exclude obvious interlopers. A prominent spike at $z = 2.095$ is clearly revealed. The histogram distribution around the spike can be well quantified by a Gaussian profile (blue dashed line) with the center z_c(Gaussian) = 2.09578 and dispersion σ_z (Gaussian) = 0.00544, or in velocity space σ_v(Gaussian) = 572 km s^{-1}. The mean of the redshift distribution within identical redshift interval is z_c(mean) = 2.09521 and standard deviation σ_z (stdev) = 0.00578, skewness = -0.2318,
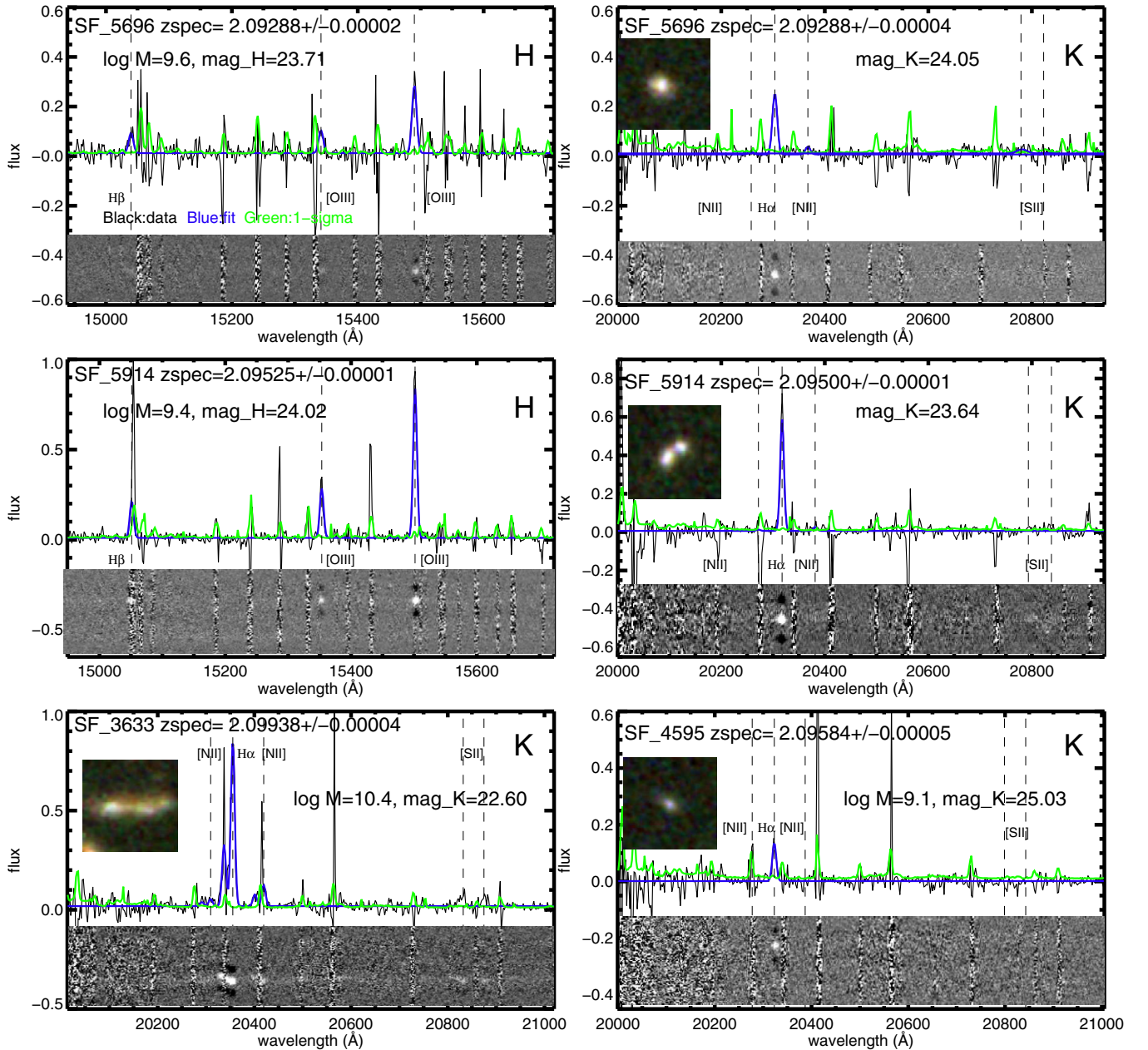
Figure 1. Examples of the flux-calibrated MOSFIRE spectra for cluster members. We select four cluster galaxies of different brightness and spectral quality that are representative of our whole sample. Cluster members are observed primarily in the K band; one-fourth of the objects have H-band observations. In each panel, the x axis is the observed wavelength in Å and the y axis is flux in units of 10^{-17} erg s^{-1} cm^2 Å^{-1}. The observed 1D spectra are presented in black and are unsmoothed; the best-fit Gaussian line profiles are superposed in blue; the 1σ error spectra are over-plotted in green. Spectroscopic redshifts from the Gaussian centroid fitting and associated statistical errors are labeled. Vertical dashed lines show the expected positions of the strong emission lines at spectroscopic redshifts. The photometric magnitude and stellar mass for each object are also marked. Embedded are $2'' \times 2''$ three color *HST* images (using the F814W, F125W, and F160W filters) obtained from the publicly available CANDELS imaging (Koekemoer et al. 2011; Grogin et al. 2011).

(A color version of this figure is available in the online journal.)

and kurtosis $= -0.1753$ consistent with a Gaussian normal distribution.

We define $z_c \pm 3*\sigma z$ as the redshift range for the cluster. There are 57 galaxies that fall in this range, of which 52 are $Q_z = 3$ objects and 5 are $Q_z = 2$ objects. Whether or not the $Q_z = 2$ galaxies are included does not change our results.

With MOSFIRE's spectral resolution and 57 confirmed members, we are able to measure for the first time a robust cluster velocity dispersion at $z \sim 2$. To calculate the cluster velocity dispersion and errors, we bootstrap (with replacement) the 57 galaxies 30000 times and ob-

tain the following: $z_c(\mathrm{boot}) = 2.09521 \pm 0.00076$ and dispersion $\sigma_z(\mathrm{boot}) = 0.00571 \pm 0.00053$, or in velocity units $\sigma_{v1D}(\mathrm{boot}) = 553 \pm 52$ km s^{-1}. To compare with previous sample sizes (typically $\sim$10 members), we randomly select 10 galaxies from our 57 members and recalculate the boot-strapped (with replacement) velocity dispersion; we obtain $\sigma_{v1D}(\mathrm{boot}) = 566 \pm 169$ km s^{-1}, i.e., the uncertainty in the velocity dispersion would be $\sim$3 times larger.

Since our spectroscopic catalog is biased toward star-forming galaxies, we are likely to have missed the quiescent/dusty galaxies or galaxies with faint emission lines below our detection
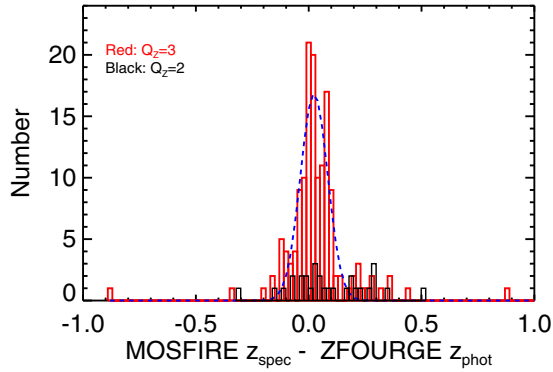
Figure 2. Histogram of the difference between our MOSFIRE spectroscopic redshifts and ZFOURGE photometric redshifts. Binsize is 0.02. Objects with $Q_z = 3$ redshift measurements (more than two emission lines identified) are shown in red and objects with $Q_z = 2$ redshift measurements (one emission line) are shown in black. Typical statistical errors for the MOSFIRE spectroscopic redshifts are 0.0001, whereas the median errors for ZFOURGE photometric redshifts are 0.05. The histogram can be well fit by a Gaussian distribution (blue dashed line). The 1σ scatter in the difference between the spectroscopic and photometric redshifts for $Q_z = 3$ objects is σ(Gaussian)/$(1.+z(=2)) \sim 2\%$.

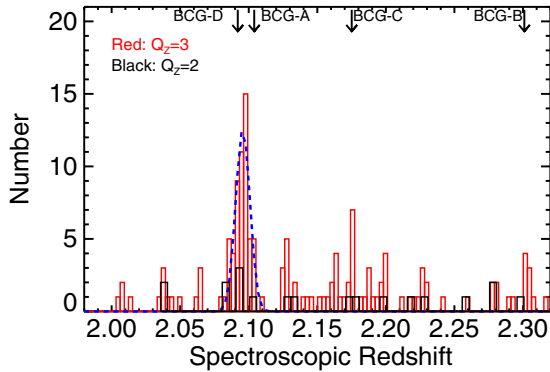(A color version of this figure is available in the online journal.)

Figure 3. Histogram for the redshift distribution of galaxies in our sample that fall in the range of $2.0 \lesssim z \lesssim 2.3$. The binsize is 0.003. $Q_z = 3$ objects are shown in red and $Q_z = 2$ in black. A strong Gaussian-shaped spike is seen at redshift $z = 2.095$. There are 57 galaxies that fall within the 3σ Gaussian width of the redshift peak. We denote those 57 galaxies as cluster members. The spectroscopic redshifts for the brightest cluster galaxies (BCG-A, B, C, D) in the over density maps of Spitler et al. (2012) are marked with downward arrows. We have confirmed BCG-A and D to be the most massive red galaxies in the $z = 2.095$ cluster, whereas BCG-B and C are most likely associated with two background structures.

(A color version of this figure is available in the online journal.)

limit (Hα 1σ flux limit of our MOSFIRE survey is 3.2×10^{-18} erg s^{-1} cm^2; SFR ~ 0.8 $M_\odot$ at $z = 2.1$ without dust correction). It has been shown that blue galaxies in clusters have a larger velocity dispersion than red galaxies (e.g., Carlberg et al. 1997). Our velocity dispersion measurement could be slightly over-estimated due to this bias. We defer the full analysis of this bias to future work.

3.2. Spatial Distribution

The spatial distribution of our MOSFIRE targets are presented in Figure 4. As described in Spitler et al. (2012), three strong overdensities (A, B, C) in this field are found by computing surface density maps in narrow $\delta z = 0.2$ redshift slices between $z = 1.5$–3.5 using the seventh nearest-neighbor metric (e.g., Papovich et al. 2010; Gobat et al. 2013). We also include another over-density region D (Figure 4) using the same algorithm (R.
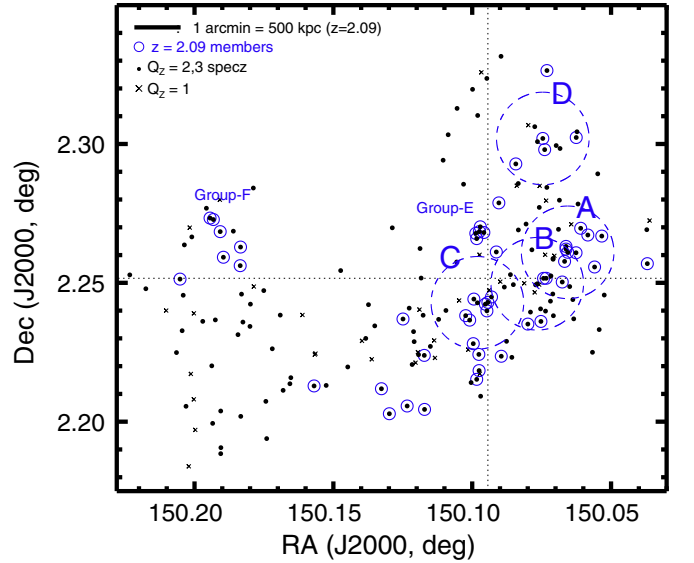

Figure 4. MOSFIRE spectroscopic redshifts in the cluster candidate field. Small black dots show the all the 180 galaxies with reliable spectroscopic redshift identifications ("$Q_z = 3$" and "$Q_z = 2$" objects). Black crosses show the 44 objects with no detections ("$Q_z = 1$" objects). Empty blue circles show the spatial distribution of the $z = 2.095$ cluster members. The dashed-line rings A, B, C, and D denote the four peaks on the seventh nearest-neighbor surface density map as labeled in Spitler et al. (2012). We adopt the brightest galaxy as an overdensity's center. The coordinates for ABC centers are the same as Spitler et al. (2012) and for D (10:00:17.739, +02:17:52.68, J2000) (R. Allen et al., in preparation). The dotted lines marked the median position of the cluster members (10:00:22.646,+02:15:05.91). The rings have a radius of 1 arcmin which corresponds to a proper scale of 500 kpc at the cluster redshift of 2.09.

(A color version of this figure is available in the online journal.)

Allen et al., in preparation). In each over-density region, massive ($M > 10^{11}$ $M_\odot$) galaxies are selected as candidate brightest cluster galaxies (BCGs). The positions of the BCGs are taken as the overdensity's centers. We also labeled in Figure 4 Groups E and F, which are groups of confirmed galaxies that are spatially concentrated and separated from the main structure.

Based on our MOSFIRE spectra, BCG-A and BCG-D are confirmed to be quiescent galaxies that show only continua. Unfortunately, our K- and H-band observations do not cover obvious stellar features for meaningful spectral template fitting. We obtain the spectroscopic redshifts for BCG-A (zspec = 2.104) and BCG-D (zspec = 2.092) from Belli et al. (2014). Our MOSFIRE spectra clearly show that BCG-B and BCG-C are star-forming emission-line galaxies that lie at redshift $z = 2.3010 \pm 0.0001$ and 2.1750 ± 0.0001, respectively. The photometric redshift of BCG-B and C is $2.15^{+0.05}_{-0.06}$ and $2.19^{+0.04}_{-0.03}$, both are under-estimated, especially for BCG-B.

The number of members with projected radius of 500 kpc for the original Spitler et al. (2012) ABC, and D overdensities are 12, 5, 8, and 4, respectively (Figure 4), though we note that what we called "BCGs" B,C are behind the main structure indicating the dangers of studying membership based solely on photometric data.

The 57 cluster members cover a total projected spatial length of $\sim 3.7 \times 5$ Mpc^2 ($\sim 7.4 \times 10$ Mpc^2 comoving). Taking the median position of the 57 cluster members (dotted lines in Figure 4) as the cluster center, we show the radial distance of members from this defined cluster center in Figure 5. Note that there are 35 members that fall within the 1.3 Mpc projected radius over the multiple over-density peaks.
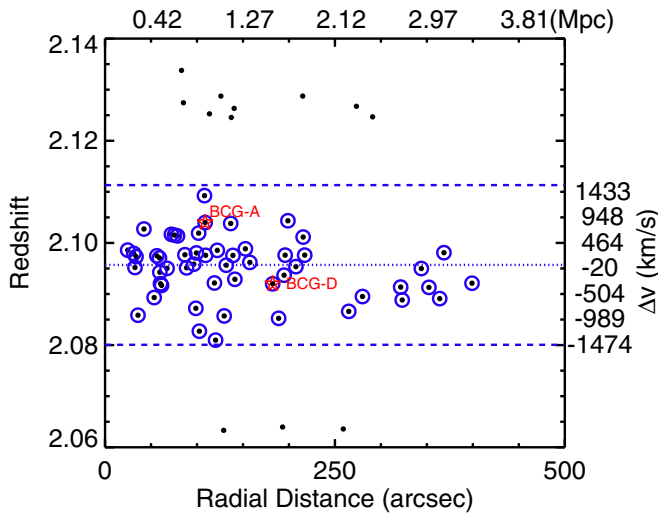
Figure 5. Spectroscopic redshift (all $Q_z = 2$, 3 objects, filled black dots) against radial distance to the "center" of the cluster defined on the median position of the cluster members. The blue horizontal lines show the positions of the redshift peak (dotted) of $z = 2.095$ and 3σ ranges (dashed). 35/57 of the members are concentrated within 1.3 Mpc of the cluster center. The positions of the two massive red galaxies BCG-A and BCG-D are highlighted in red stars. The velocities with respect to the cluster redshift $z = 2.095$ are labeled on the y axis on the right.

(A color version of this figure is available in the online journal.)

4. COMPARISON WITH SIMULATIONS

To help us understand what our observed structure at $z = 2.095$ should evolve into at $z = 0$, we employ the 2160^3 particle Gpc volume (particle mass $m_p = 1.1 \times 10^{10} \, M_\odot$) GiggleZ-main simulation (Poole et al. 2014). We have computed 1D velocity dispersions for all the friends-of-friends (FoF) structures of the simulation at $z = 0$ and $z = 2.2$ (the closest snapshot to our observed redshift) using substructures exceeding $M_{\rm vir} = 4.3 \times 10^{11} \, M_\odot$. Merger trees were used to determine what each $z = 2.2$ FoF structure evolves into at $z = 0$. We find that systems with velocity dispersions in the range $\sigma_{\rm 1D} = 552 \pm 52$ km s^{-1} at $z = 2.2$ have virial masses in the range $M_{\rm vir} = 10^{13.5 \pm 0.2} \, M_\odot$ and that they evolve into systems with $M_{\rm vir} = 10^{14.4 \pm 0.3} \, M_\odot$ and $\sigma_{\rm 1D} = 680^{+73}_{-110}$ km s^{-1} (all ranges are 68% confidence), in agreement with a Virgo-like cluster (de Vaucouleurs 1961). Two hundred ninety-nine such systems are found in the simulation suggesting an incidence of one per 2.5 square degrees over the redshift range $z = 2.0$ to 2.3. This corresponds to a ~4% occurrence of such a cluster in the original ZFOURGE survey area of 0.1 deg^2.

These results are in good agreement with the $z = 2\, \sigma_{\rm sub} - M_{\rm vir}$ relation of Munari et al. (2013) and with the results of Chiang et al. (2013), whose simulations indicate that a $10^{13.5} \, M_\odot$ system should evolve to a mass of ~$10^{14.5} \, M_\odot$ at $z = 0$.

5. CONCLUSIONS

We carry out MOSFIRE spectroscopic observations in the $z \sim 2$ galaxy cluster candidate with a red-sequence that was first discovered from the Magellan/FOURSTAR Galaxy Evolution Survey (ZFOURGE) (Spitler et al. 2012). This galaxy cluster was identified using rest-frame optical and NIR imaging and is thus an important link between the UV-selected systems at this epoch (e.g., Steidel et al. 2005; Digby-North et al. 2010) and massive clusters at lower redshifts (e.g., Gal & Lubin 2004). Our successful spectroscopic campaign confirms the accuracy

of the photometric redshifts derived from ZFOURGE's deep medium-bandwidth photometry.

By combining MOSFIRE's spectral capabilities with our efficient selection of $z \sim 2$ targets, we are able to identify cluster members and accurately measure the cluster's kinematics. We measure spectral redshifts for 180 objects and identify 57 cluster members that have a mean redshift of $z = 2.095$. The redshifts for cluster members are determined primarily from Hα and [N II] emission, and the cluster velocity dispersion is $\sigma_{\rm v1D} = 552 \pm 52$ km s^{-1}. Most of the cluster galaxies (35) lie within a region with a projected radius of 1.3 Mpc.

This is the first study of a galaxy cluster at $z \geqslant 2.0$ with the combination of spectral resolution (~26 km s^{-1}) and the number of confirmed members (>50) needed to study cluster kinematics robustly and map members over a large field of view (12×12 arcmin^2). Our accurate velocity dispersion measurement of this clustering structure allows us to use simulations to trace the cluster's likely evolution to $z = 0$. Our simulation results show that the ZFOURGE cluster at $z = 2.095$ should evolve into a Virgo-like system locally with $M_{\rm vir} = 10^{14.4 \pm 0.3} \, M_\odot$.

Our results show that galaxy clusters at $z \sim 2$ can now be studied in the same detailed manner as clusters at $z \lesssim 1$. However, unlike galaxies in massive clusters at $z \sim 0$, the ZFOURGE cluster members show a wealth of Hα emission and other signs of star formation activity. Our next work will report the mass–metallicity relation, ionization parameter evolution, and other physical properties of the ZFOURGE cluster at $z = 2.095$.

REFERENCES

Belli, S., Newman, A. B., Ellis, R. S., & Konidaris, N. P. 2014, ApJL, 788, L29
Brodwin, M., Stanford, S. A., Gonzalez, A. H., et al. 2013, ApJ, 779, 138
Carlberg, R. G., Yee, H. K. C., Ellingson, E., et al. 1997, ApJL, 476, L7
Chiang, Y.-K., Overzier, R., & Gebhardt, K. 2013, ApJ, 779, 127
Chiang, Y.-K., Overzier, R., & Gebhardt, K. 2014, ApJL, 782, L3
de Vaucouleurs, G. 1961, ApJS, 6, 213
Digby-North, J. A., Nandra, K., Laird, E. S., et al. 2010, MNRAS, 407, 846
Dressler, A. 1980, ApJ, 236, 351
Gal, R. R., & Lubin, L. M. 2004, ApJL, 607, L1
Galametz, A., Stern, D., Pentericci, L., et al. 2013, A&A, 559, A2
Gobat, R., Strazzullo, V., Daddi, E., et al. 2013, ApJ, 776, 9
Grogin, N. A., Kocevski, D. D., Faber, S. M., et al. 2011, ApJS, 197, 35
Hayashi, M., Kodama, T., Tadaki, K.-i., Koyama, Y., & Tanaka, I. 2012, ApJ, 757, 15
Henry, J. P., Aoki, K., Finoguenov, A., et al. 2014, ApJ, 780, 58
Hogg, D. W., Blanton, M. R., Brinchmann, J., et al. 2004, ApJL, 601, L29

Hopkins, A. M., & Beacom, J. F. 2006, ApJ, 651, 142
Koekemoer, A. M., Faber, S. M., Ferguson, H. C., et al. 2011, ApJS, 197, 36
Kurk, J. D., Pentericci, L., Overzier, R. A., Röttgering, H. J. A., & Miley, G. K. 2004, A&A, 428, 817
Lee, K.-S., Dey, A., Hong, S., et al. 2014, arXiv:1405.2620
McCarthy, P. J., Yan, H., Abraham, R. G., et al. 2007, ApJL, 664, L17
McLean, I. S., Ramsay, S. K., & Takami, H. 2010, Proc. SPIE, 7735, 77351E-1
McLean, I. S., Steidel, C. C., Epps, H. W., et al. 2012, Proc. SPIE, 8446, 84460J
Munari, E., Biviano, A., Borgani, S., Murante, G., & Fabjan, D. 2013, MNRAS, 430, 2638
Muzzin, A., Wilson, G., Demarco, R., et al. 2013, ApJ, 767, 39
Newman, A. B., Ellis, R. S., Andreon, S., et al. 2014, ApJ, 788, 51
Papovich, C., Momcheva, I., Willmer, C. N. A., et al. 2010, ApJ, 716, 1503

Persson, S. E., Murphy, D. C., Smee, S., et al. 2013, PASP, 125, 654
Poole, G. B., Blake, C., Marin, F. A., et al. 2014, arXiv:1407.0390
Rettura, A., Rosati, P., Nonino, M., et al. 2010, ApJ, 709, 512
Shimakawa, R., Kodama, T., Tadaki, K.-i., et al. 2014, MNRAS, 441, L1
Spitler, L. R., Labbé, I., Glazebrook, K., et al. 2012, ApJL, 748, L21
Spitler, L. R., Straatman, C. M. S., Labbé, I., et al. 2014, ApJL, 787, L36
Stanford, S. A., Brodwin, M., Gonzalez, A. H., et al. 2012, ApJ, 753, 164
Steidel, C. C., Adelberger, K. L., Shapley, A. E., et al. 2005, ApJ, 626, 44
Steidel, C. C., Rudie, G. C., Strom, A. L., et al. 2014, arXiv:1405.5473
Strazzullo, V., Gobat, R., Daddi, E., et al. 2013, ApJ, 772, 118
Tomczak, A. R., Quadri, R. F., Tran, K.-V. H., et al. 2014, ApJ, 783, 85
Tran, K.-V. H., Papovich, C., Saintonge, A., et al. 2010, ApJL, 719, L126
Zeimann, G. R., Stanford, S. A., Brodwin, M., et al. 2012, ApJ, 756, 115